1999

A Mathematical Model of an Electrochemical Capacitor with Double-Layer and Faradaic Processes

Chuan Lin
University of South Carolina - Columbia

James A. Ritter
University of South Carolina - Columbia

Branko N. Popov
University of South Carolina - Columbia, popov@engr.sc.edu

Ralph E. White
University of South Carolina - Columbia, white@cec.sc.edu

Publication Info

Journal of the Electrochemical Society, 1999, pages 3168-3175.

Publisher's link: http://dx.doi.org/10.1149/1.1392450
DOI: 10.1149/1.1392450

Journal of The Electrochemical Society, **146** (9) 3168-3175 (1999)
S0013-4651(98)11-057-1 CCC: $7.00

A Mathematical Model of an Electrochemical Capacitor with Double-Layer and Faradaic Processes

Chuan Lin, James A. Ritter,* Branko N. Popov,* and Ralph E. White*,z

Department of Chemical Engineering, Swearingen Engineering Center, University of South Carolina, Columbia, South Carolina 29208, USA

A mathematical model of an electrochemical capacitor with hydrous ruthenium oxide ($RuO_2 \cdot xH_2O$) electrodes including both double-layer and surface faradaic processes is developed to predict the behavior of the capacitor under conditions of galvanostatic charge and discharge. The effect of $RuO_2 \cdot xH_2O$ particle size is studied and shows that the smaller the particles the better the performance because of the increased surface area per unit volume or mass. The model also predicts that the faradaic process increases significantly the energy per unit volume of the capacitor for power densities of 100 kW/L or less.

Manuscript submitted November 16, 1998; revised manuscript received April 28, 1999.

Electrochemical capacitors have been receiving increased attention during recent years[1-5] as high-power devices in energy-storage systems. There are two mechanisms of energy storage in electrochemical capacitors: (*i*) a double-layer (DL) charging process due to charge separation, and (*ii*) a faradaic process due to redox reactions. Devices based on the DL phenomenon are referred to as electrochemical DL capacitors, and those based on faradaic reactions are termed pseudocapacitors. Very high-surface-area carbon materials[6-9] are widely used for DL capacitors. On the other hand, relatively high-surface-area transition metal oxides, such as amorphous $RuO_2 \cdot xH_2O$, [10] porous NiO_x, [11,12] and CoO_x, [12,13] have been identified as possible electrode materials for pseudocapacitors.

A number of models have been developed for analyzing the behavior of DL capacitors. Posey and Morozumi[14] developed a model for potentiostatic and galvanostatic charging of the DL in porous electrodes. Johnson and Newman[15] also developed a model for a porous electrode to analyze desalting processes in terms of ionic adsorption on porous carbon, and Tiedemann and Newman[16] used the results from that model to evaluate the DL capacity of porous electrodes. Recently, Srinivasan *et al.*[17] developed an analytic model and used it to study constant-current discharging, cyclic voltage sweeping, and the ac impedance of carbon xerogel DL capacitors. Also, an analytic model was developed by Farahmandi[18] and used to study the effects of both ionic and solid-phase conductivities on the behavior of an electrochemical capacitor. More recently, Pillay and Newman[19] modeled the influence of side reactions on the performance of electrochemical capacitors. However, none of these capacitor models accounted for both pseudocapacitance and DL capacitance. In fact, few capacitor models have considered faradaic reactions, and for those that did,[20,21] only the approximation of linear faradaic kinetics was considered.

Therefore, the objective of this work is to develop a mathematical model of an electrochemical capacitor with both DL and faradaic processes. These two capacitive processes can occur simultaneously with both contributing to the overall capacitance of the material. This is especially true in the relatively high-surface area transition metal oxide pseudocapacitor materials.[5] The specific system used to illustrate the complementary effects of DL and faradaic processes is a symmetric capacitor comprised of uniformly sized spherical hydrous ruthenium oxide ($RuO_2 \cdot xH_2O$) particles with 30 wt % sulfuric acid as the electrolyte. In the model, the diffusion of protons into the solid $RuO_2 \cdot xH_2O$ particles is ignored for simplicity; consequently, the DL and faradaic processes take place only on the external surface of the particles. This simplification can be removed, however, by following the procedure presented by Doyle *et al.*[22] for ionic diffusion in the particles. The effects of particle size and cell current density on the charge/discharge behavior are studied, and the roles of the DL and Faradaic processes are delineated with specific reference to Ragone plots.

Model Description

Figure 1 displays a schematic of a typical capacitor cell. Two identical $RuO_2 \cdot xH_2O$ electrodes are separated by an ionically conductive glass fiber and are contacted on one side, as shown in Fig. 1, with tantalum current collectors. A solution of 30 wt % H_2SO_4 is used as the electrolyte, which completely fills the pores in the electrodes and the separator. A one-dimensional model is developed using the macrohomogeneous theory of porous electrodes, reviewed by Newman and Tiedemann,[23] and De Vidts and White.[24] In the model presented here, the electrolyte concentration is assumed to be invariant and side reactions and thermal effects are ignored, along with the variation of the DL capacitance with potential.

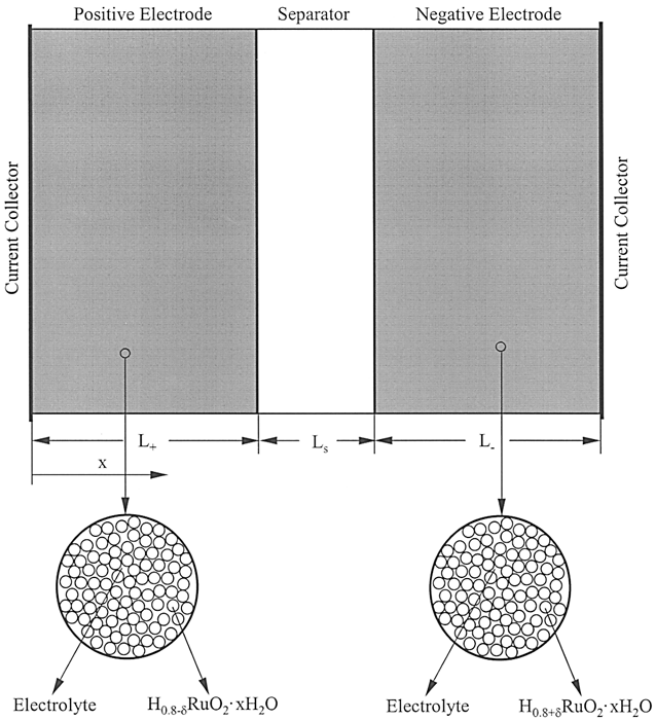

Figure 1. Schematic of an electrochemical capacitor cell upon which the model is based.

* Electrochemical Society Active Member.
z E-mail: rew@sc.edu

S0013-4651(98)11-057-1 CCC: $7.00

The faradaic reactions occurring in the electrodes during charge/discharge are expressed as[25]

$$H_{0.8}RuO_2{\cdot}xH_2O \underset{\text{discharge}}{\overset{\text{charge}}{\rightleftharpoons}} H_{0.8-\delta}RuO_2{\cdot}xH_2O + \delta H^+ + \delta e^- \quad [1]$$

for the positive electrode, and as

$$H_{0.8}RuO_2{\cdot}xH_2O + \delta H^+ + \delta e^- \underset{\text{discharge}}{\overset{\text{charge}}{\rightleftharpoons}} H_{0.8+\delta}RuO_2{\cdot}xH_2O \quad [2]$$

for the negative electrode, where the state of charge, δ, is 0.5 for a cell to be charged to 1 V. These reactions show that initially the active materials in both electrodes are $H_{0.8}RuO_2{\cdot}xH_2O$, which may be obtained by discharging each $RuO_2{\cdot}xH_2O$ electrode separately using external electrodes. Then, during charge, the oxidation reaction (Eq. 1) takes place in the positive electrode and the reduction reaction (Eq. 2) occurs in the negative electrode. Finally, during discharge, the opposite reactions take place in both electrodes, which brings both electrodes to their original states after full discharge, thereby completing a charge/discharge cycle. Thus, during charge, the oxidation state of Ru changes from 3.2 to 3.7 in the positive electrode and from 3.2 to 2.7 in the negative electrode, and during discharge, it changes back from 3.7 to 3.2 in the positive electrode and from 2.7 to 3.2 in the negative electrode.

In an electrode, the total current transferred from the matrix phase to the electrolyte phase is expressed in terms of the DL current and the faradaic current as[19,26]

$$\frac{\partial i_2}{\partial x} = s_v C_d \frac{\partial(\Phi_1 - \Phi_2)}{\partial t} + s_v j_f \quad [3]$$

where i_2 is the superficial current density based on the projected electrode area in the electrolyte phase, x is the position coordinate, s_v is the specific surface area per unit volume of the electrode, C_d is the DL capacitance, Φ_1 and Φ_2 are the potentials in the matrix and electrolyte phases, respectively, and j_f is the faradaic transfer current density. Φ_2 is defined as the potential[19,25] of a saturated calomel reference electrode (SCE) connected to the electrolyte phase at the position of interest relative to an identical electrode connected to the electrolyte phase just inside the left current collector ($x = 0$). Thus, Φ_2 is zero at $x = 0$. The faradaic transfer current, j_f, is taken in the form of the Butler-Volmer equation[27]

$$j_f = i_0\{\exp[\alpha_a f(\Phi_1 - \Phi_2 - U_1)] - \exp[-\alpha_c f(\Phi_1 - \Phi_2 - U_1)]\} \quad [4]$$

where i_0 is the exchange current density of the faradaic reaction, f is equal to F/RT, F is Faraday's constant, R is the universal gas constant, T is the absolute temperature, α_a and α_c are the anodic and cathodic transfer coefficients for the reactions, respectively, and U_1 is the equilibrium potential of the faradaic reaction. U_1 is a function of the state of charge,[25] which can be expressed by θ, the fraction of oxidized species in the electrode. By introducing another variable, Q_f, the faradaic charge of the electrode, δ, θ, and j_f are related by the following equations

$$\theta = \frac{Q_f - Q_{f,red}}{Q_{f,oxd} - Q_{f,red}} \quad [5]$$

$$\delta = 0.5\theta \quad [6]$$

$$\frac{\partial Q_f}{\partial t} = s_v j_f \quad [7]$$

where $Q_{f,red}$ is the faradaic charge of a fully reduced electrode, and $Q_{f,oxd}$ is the faradaic charge of a fully oxidized electrode. Equation 7 relates the rate of accumulation of the faradaic charge within the electrode to the faradaic transfer current. For simplicity, Eq. 4, 5, and 7 are combined into a single equation

$$\frac{\partial\theta}{\partial t} = \frac{s_v i_0}{Q_{f,oxd} - Q_{f,red}}\{\exp[\alpha_a f(\Phi_1 - \Phi_2 - U_1)] - \exp[-\alpha_c f(\Phi_1 - \Phi_2 - U_1)]\} \quad [8]$$

Conservation of charge leads to

$$\frac{\partial i_1}{\partial x} + \frac{\partial i_2}{\partial x} = 0 \quad [9]$$

where i_1 is the superficial current density based on the projected electrode area in the matrix phase of the porous electrode. With the assumption of no concentration gradients in the electrodes, Ohm's law applies in both the matrix and electrolyte phases as

$$i_1 = -\sigma\frac{\partial\Phi_1}{\partial x} \quad [10]$$

$$i_2 = -\kappa_p\frac{\partial\Phi_2}{\partial x} \quad [11]$$

where σ is the electronic conductivity of the matrix, and κ_p is the ionic conductivity of the electrolyte inside the pores of the electrodes. In order to solve the system of equations more efficiently, Eq. 3, 4, 9, 10, and 11 are combined into a single equation

$$\frac{\partial^2 E}{\partial\xi^2} = \tau\frac{\partial E}{\partial t} + \frac{\tau i_0}{C_d}\{\exp[\alpha_a f(E - U_1)] - \exp[-\alpha_c f(E - U_1)]\} \quad [12]$$

with the local electrode potential, E, defined as

$$E = \Phi_1 - \Phi_2 \quad [13]$$

and the DL time constant as

$$\tau = s_v C_d L^2\left(\frac{1}{\sigma} + \frac{1}{\kappa_p}\right) \quad [14]$$

where L is the thickness of one electrode ($L = L_+ = L_-$), and the dimensionless distance ξ is defined as x/L. In the separator, because the electronic conductivity in the glass fiber is zero

$$i_1 = 0 \quad [15]$$

and thus the total transfer current is zero

$$\frac{\partial i_2}{\partial x} = 0 \quad [16]$$

However, Ohm's law still applies to the current in the electrolyte within the pores of the separator, as

$$i_2 = -\kappa_s\frac{\partial\Phi_2}{\partial x} \quad [17]$$

where κ_s is the ionic conductivity in the pores of the separator.

To solve this system of partial differential and algebraic equations, the following boundary and initial conditions are used. For the case of a constant-current charge/discharge between 0 and 1 V, the boundary conditions for the positive electrode are

$$\text{at } \xi = 0,\ t > 0 \qquad \frac{\partial E}{\partial\xi} = -\frac{i_{cell}L}{\sigma} \quad [18]$$

$$\frac{\partial\theta}{\partial t} = \frac{s_v i_0}{Q_{f,oxd} - Q_{f,red}}\{\exp[\alpha_a f(E - U_1)] - \exp[-\alpha_c f(E - U_1)]\} \quad [19]$$

$$\text{at } \xi = 1,\ t > 0 \qquad \frac{\partial E}{\partial\xi} = -\frac{i_{cell}L}{\kappa_p} \quad [20]$$

S0013-4651(98)11-057-1 CCC: $7.00

$$\frac{\partial\theta}{\partial\xi} = 0 \quad [21]$$

The boundary conditions are set such that at the interface between the current collector and the electrode ($\xi = 0$), the current arises from the matrix phase, and at the interface between the electrode and separator ($\xi = 1$), the current arises from the solution phase. The initial conditions are[25]

$$\text{at } t = 0 \text{ for charge} \quad E = V_o \text{ and } \theta = 0 \quad [22]$$

$$\text{at } t = 0 \text{ for discharge} \quad E = 2V_o \text{ and } \theta = 1 \quad [23]$$

where V_o is the initial potential before charge and is taken as 0.5 V (SCE) for a cell charge/discharge between 0 and 1 V. Similar boundary and initial conditions can be set for the negative electrode. However, in this model only the positive electrode is simulated; because of the symmetrical feature of the two electrodes, results for the negative electrode are calculated based on the simulation results for the positive electrode.

The entire system of equations to be solved is comprised of two equations and two unknowns, which are Eq. 8 and 12, and E and θ, respectively. The system of equations for the positive electrode is solved using a backward finite difference method[28] with Newman's BAND(J) algorithm.[29] It is noteworthy that Eq. 17 is used to evaluate the potential in the solution phase of the separator, which is also solved simultaneously with the system of equations for the positive electrode. Once E and θ are obtained, the other unknowns are calculated using these above equations; for example, Eq. 11, 13, and 4 are used to calculate Φ_1, Φ_2, and j_f, respectively. The DL and faradaic currents in each electrode are defined by and obtained from the following two equations, respectively

$$i_c = -s_v C_d \frac{\partial E}{\partial t} \quad [24]$$

$$i_f = -s_v j_f \quad [25]$$

Model Parameters

In this study, the $RuO_2 \cdot xH_2O$ particles are assumed to be nonporous spheres with a uniform size; thus, the pores in the electrodes are composed of the spaces between the particles, and the surface area per unit volume, s_v, of the electrode is expressed as

$$s_v = \frac{6(1-\epsilon)}{D} \quad [26]$$

where D is the diameter of the particles and ϵ is the electrode porosity (taken as 0.25). Many of the other parameters associated with the $RuO_2 \cdot xH_2O$ are unavailable in the literature; therefore, the following reasonable assumptions are made. The DL capacitance on the RuO_2 surface is assumed to be 2.0×10^{-5} F/cm^2, which is the same for carbon materials.[30] Both of the anodic and cathodic transfer coefficients, α_a and α_c, are taken as 0.5; and the exchange current density of the faradaic reactions, i_0, is taken as 10^{-5} A/cm^2. The equilibrium potential, U_1, for the faradaic reactions is estimated from a linear relationship between the potential and the state of charge (δ), as reported by Jow and Zhang.[25] At $\delta = 0$, U_1 is equal to 0.5 V for both the electrodes, and at $\delta = 0.5$, U_1 is equal to 1 and 0 V for the positive and negative electrodes, respectively. Also, according to the relationship between δ and θ (Eq. 6), U_1 is equal to $0.5(1 + \theta)$ and 0.5θ for the reactions in the positive (Eq. 1) and negative electrodes (Eq. 2), respectively. Here θ is the fraction of oxidized species in the faradaic reaction.

In addition, it is assumed that the faradaic reactions take place only on the surface of the $RuO_2 \cdot xH_2O$ particles inside the electrodes. As a result, the faradaic charge of a fully oxidized electrode, $Q_{f,oxd}$, is estimated from

$$Q_{f,oxd} = \frac{s_v \delta F}{h^2 L_A} \quad [27]$$

where s_v is obtained from Eq. 26, δ is equal to 0.5 for the fully charged cell, h is the length of the crystal lattice on the surface and taken approximately as 4 Å,[31] and L_A is Avogadro's number. Equation 27 implies that there is only one Ru atom in the area of h^2 on the surface of the $RuO_2 \cdot xH_2O$ particles and that $Q_{f,oxd}$ is a function of the particle size. The faradaic charge of a fully reduced electrode, $Q_{f,red}$, is taken as zero.

The electronic conductivity of the matrix, σ, is taken as 10^5 S/cm, [32] and the ionic conductivity of bulk 30 wt % H_2SO_4, κ_0, is 0.8 S/cm. [33] The ionic conductivity of the electrolyte inside the pores of the electrode is frequently expressed as[29]

$$\kappa_p = \kappa_0 \epsilon^{1.5} \quad [28]$$

Similarly, the ionic conductivity of the electrolyte inside the pores of the separator is given by

$$\kappa_s = \kappa_0 \epsilon_s^{1.5} \quad [29]$$

where the separator porosity, ϵ_s, is taken as 0.7. The electrode thickness for both the positive and negative electrodes is 50 μm, the separator thickness is 25 μm, and the temperature is 25°C. All these values are summarized in Tables I and II, along with the values of other parameters used in this model.

Results

At the outset, it is useful to verify the accuracy of the numerical method, which is done by comparing the numerical results for the

Table I. Model parameters that describe the Faradaic kinetics and open-circuit potentials of the electrodes.

Parameter	Value	Reference
i_0	10^{-5} A/cm^2	Assumed
α_a	0.5	Assumed
α_c	0.5	Assumed
U_1 (positive electrode)	$0.5(1 + \theta)$ V (*vs.* SCE)	Jow and Zhang[25]
U_1 (negative electrode)	0.5θ V (*vs.* SCE)	Jow and Zhang[25]

Table II. Model parameters that describe the electrodes and separator.

Parameter	Value	Reference
D	5, 10, 30 nm	Assumed
ϵ	0.25	Assumed
ϵ_s	0.7	Pillay and Newman[19]
$L = L_+ = L_-$	5×10^{-3} cm	Assumed
L_s	2.5×10^{-3} cm	Assumed
C_d	2×10^{-5} F/cm^2	Assumed
s_v	1.5×10^6, 4.5×10^6, and 9.0×10^6 cm^2/cm^3 for the particle sizes of D = 30, 10, and 5 nm, respectively	From Eq. 26
h	4.0×10^{-8} cm	Pollak and O'Grady[31]
$Q_{f,oxd}$	150.2, 450.6, and 901.2 C/cm^3 for the particle sizes of D = 30, 10, and 5 nm, respectively	From Eq. 27
$Q_{f,red}$	0	Assumed
σ	10^5 S/cm	Trasatti and Lodi[32]
κ_0	0.8 S/cm	Darling[33]
κ_p	0.1 S/cm	From Eq. 28
κ_s	0.469 S/cm	From Eq. 29
T	298.15 K	Assumed
τ	7.5×10^{-3}, 2.25×10^{-2}, 4.5×10^{-2} s for the particle sizes of D = 30, 10, and 5 nm, respectively	From Eq. 14
V_o	0.5 V (*vs.* SCE)	Assumed

S0013-4651(98)11-057-1 CCC: $7.00

DL process alone (*i.e.*, faradaic process is shut off) with those generated from a completely analytical model for DL capacitors developed by Srinivasan *et al.*[17] Some dimensionless variables are also introduced, such as dimensionless cell potential, Φ^*_{cell}, dimensionless local potential, E^*, dimensionless time, τ^*, dimensionless cell current, i^*_{cell}, etc. The definitions of these dimensionless variables are given in the List of Symbols. Finally, the results presented here are for discharge only, because the results for charge are simply the mirror image of those for discharge.

Figure 2A, B, and C compares the results for the change in the dimensionless cell potential with time at two different cell currents, the dimensionless potential distribution at different discharge times, and the dimensionless DL current distribution at different discharge times, respectively. In Fig. 2A, the dimensionless cell potential, Φ^*_{cell}, is defined as $\Phi_{cell}/2V_o$, where Φ_{cell} represents the matrix potential difference between the two current collectors. Also, the relative utilization,[17] $\tau^* i^*_{cell}$, represents the fraction of the available capacity extracted from the cell. The $RuO_2 \cdot xH_2O$ particles are 5 nm in diameter. The results show that the numerical solutions agree very well with the analytical solutions up to the fourth digit, which is sufficient for numerical simulations. It is noteworthy that this numerical accuracy is achieved by taking 101 space node points and a time step of 10^{-6} s up to 2 s and 10^{-4} s thereafter. All of the results presented were obtained from the numerical model using these discretization grid sizes.

Figure 3A shows discharge curves for the combined DL and faradaic processes at a constant cell current of $i^*_{cell} = 0.001$ for three different $RuO_2 \cdot xH_2O$ particle sizes, and Fig. 3B compares the discharge behavior of each of their contributions for a capacitor with 5 nm diam $RuO_2 \cdot xH_2O$ particles at a constant cell current of $i^*_{cell} = 0.001$ to examine how the DL and faradaic processes separately affect the cell potential. Linear relationships of the cell potential with discharge time are observed in Fig. 3A for all three particle

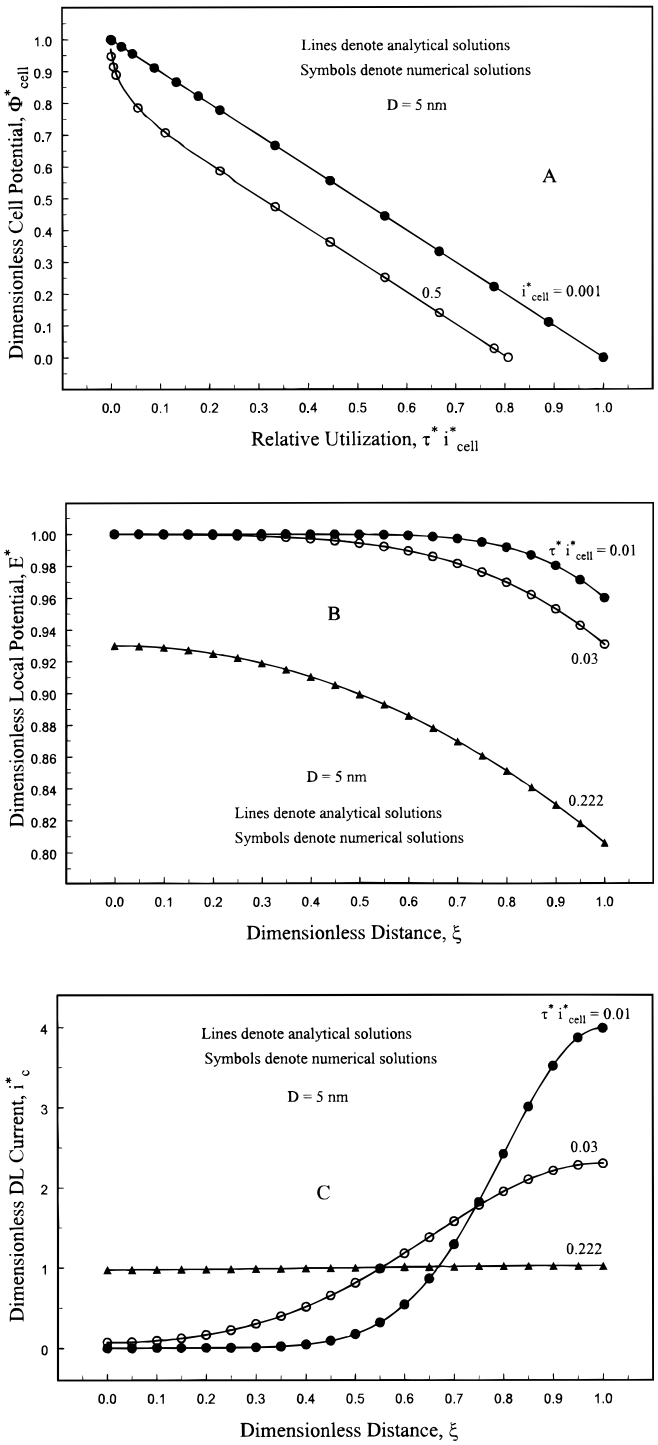

Figure 2. Comparisons of the numerical solutions with the analytic ones for the DL process alone and 5 nm diam $RuO_2 \cdot xH_2O$ particles: (A) constant-current discharge curves at two dimensionless currents; (B) potential distribution through the positive electrode at different times during discharge at a constant current of $i^*_{cell} = 0.5$; and (C) DL current distribution through the positive electrode at different times during discharge at a constant current of $i^*_{cell} = 0.5$.

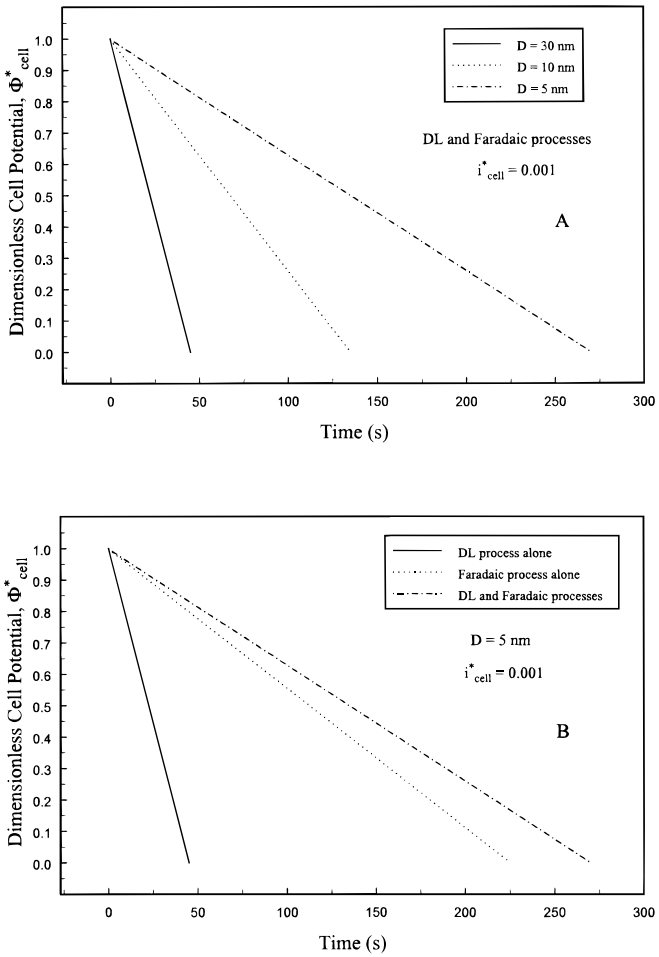

Figure 3. (A) Effect of $RuO_2 \cdot xH_2O$ particle size on constant-current discharge behavior for the combined DL and faradaic processes at $i^*_{cell} = 0.001$ and (B) comparison of constant-current discharge behavior for the DL process alone, faradaic process alone, and combined DL and faradaic processes at $i^*_{cell} = 0.001$ and with 5 nm diam $RuO_2 \cdot xH_2O$ particles.

S0013-4651(98)11-057-1 CCC: $7.00

sizes, and the discharge time increases with a decrease in the particle size. The actual discharge time is used here instead of relative utilization ($\tau^* i^*_{cell}$), because the DL time constant (τ) depends on the particle size, which makes the discharge curves incomparable in terms of relative utilization. Linear relationships are again observed in Fig. 3B for the DL process alone, faradaic process alone, and the combined DL and faradaic processes; and the DL process alone has the shortest discharge time, the faradaic process alone has a discharge time five times longer than the DL process alone, and the combined DL and faradaic processes has the longest discharge time, appearing as a linear combination of the two individual processes. The linear behavior of the change in cell potential with time is characteristic of a DL capacitor when the DL capacitance is independent of the potential. As for the faradaic process simulated here, the linear behavior is most likely due to the linear relationship between the equilibrium potential and the state of charge, which makes this faradaic material of $RuO_2 \cdot xH_2O$ behave like a simple DL capacitor.

Figure 4A and B illustrates the effect of cell current on the cell potential for the combined DL and faradaic processes and for the faradaic process alone, respectively. The $RuO_2 \cdot xH_2O$ particles are 5 nm in diam. For the combined DL and faradaic processes (Fig. 4A), at the smaller current (*i.e.*, $i^*_{cell} = 0.001$), the cell potential decreases linearly with time. However, at the larger current (*i.e.*, $i^*_{cell} = 0.5$), a sharp drop in potential at the start of discharge is observed, which is followed by a linear decrease in potential for the remainder of the discharge. These discharge curves are similar in shape to those for the DL process alone, as shown in Fig. 2A, but the potential drop is larger for the combined DL and faradaic processes. For the faradaic process alone (Fig. 4B), at the smaller current, the cell potential also decreases linearly as those observed for the combined DL and faradaic processes (Fig. 4A) and for the DL process alone (Fig. 2A). At the larger current, however, the cell potential behaves differently from that for the DL process alone. The potential decreases almost linearly with time but with a marked drop at the start of discharge, unlike the initial potential drops for the DL process alone that exhibit curvature. This marked potential drop is believed to be associated with the faradaic kinetic resistance; the result is consistent with a larger drop in potential for the combined DL and faradaic processes than that for the DL process alone.

To examine how potentials and currents inside the electrode change during discharge, the distributions of the potential throughout the positive electrode at different discharge times at a cell current of $i^*_{cell} = 0.5$ are shown in Fig. 5A and B for the combined DL and faradaic processes and for the faradaic process alone, respectively. The corresponding distributions of the currents are illustrated in Fig. 6A and B for the combined DL and faradaic processes and in Fig. 6C for the faradaic process alone. For the combined DL and faradaic processes (Fig. 5A), the potential distribution changes gradually from the initial uniform distribution at the start of discharge to a steady-state nonuniform profile at about $\tau^* i^*_{cell} = 0.222$. Then the cell potential decreases with this steady-state profile until the cell is totally discharged. The nonuniform potential distribution is due mainly to the ohmic potential drop in the solution phase (the conductivity in the matrix phase is much greater than that in the solution phase in this modeling simulation), and the transition time to reach the steady-state profile is determined by the DL time constant.

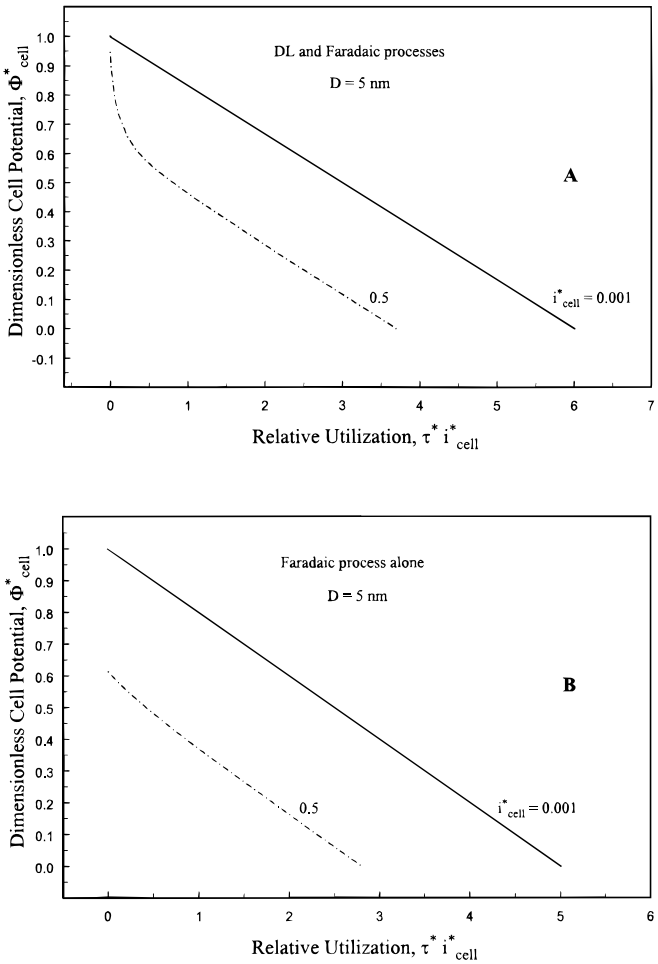

Figure 4. Constant-current discharge curves at two dimensionless currents: (A) for the combined DL and faradaic processes and (B) for the faradaic process alone.

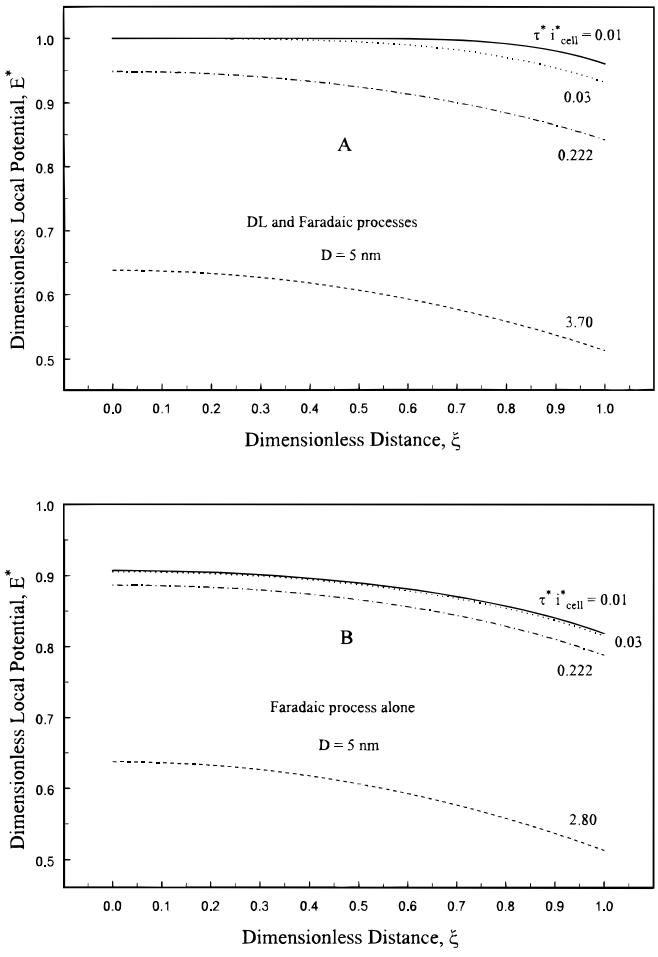

Figure 5. Potential distributions throughout the positive electrode at different times during discharge at a constant current of $i^*_{cell} = 0.5$: (A) for the combined DL and faradaic processes and (B) for the faradaic process alone.

S0013-4651(98)11-057-1 CCC: $7.00 © The Electrochemical Society, Inc.

Again, these distributions are similar in shape to those at the same discharge times for the DL process alone, as shown in Fig. 2B, but the decrease in potential is slower for the combined DL and faradaic processes because it holds more energy compared with the DL process alone. For the faradaic process alone (Fig. 5B), the potential distribution changes immediately to a steady-state nonuniform profile after the start of the discharge, then the potential decreases with this profile until the cell is fully discharged. The reason for this immediate change in potential distribution is that in this case there is no DL time constant that controls the transition of the potential distribution to gradually reach a steady-state profile. Again, the nonuniform potential distribution is largely due to the ohmic resistance in the solution phase.

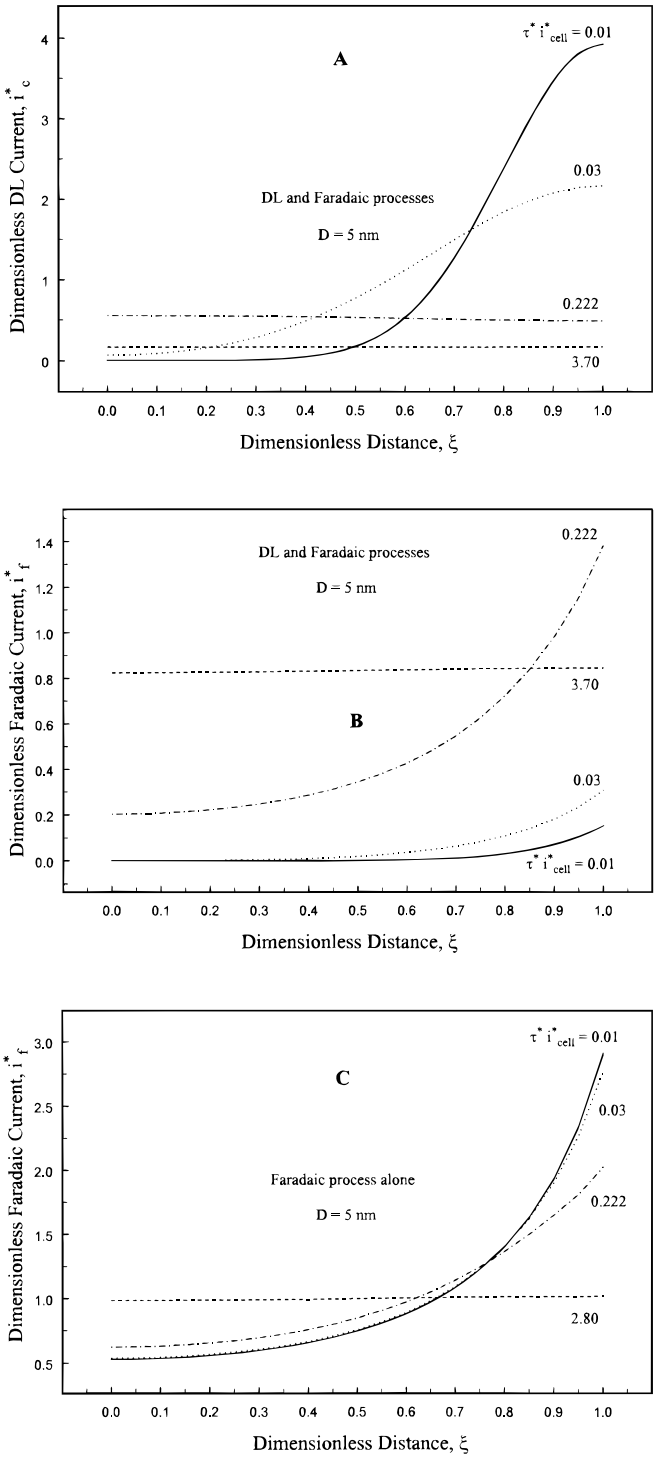

Figure 6. Current distributions throughout the positive electrode at different times during discharge at a constant current of $i^*_{cell} = 0.5$: (A) and (B) for the combined DL and faradaic processes, and (C) for the faradaic process alone.

For the combined DL and faradaic processes, the DL current distribution throughout the electrode (Fig. 6A) is very nonuniform at short times, and the degree of this nonuniformity decreases with time. The DL current attains a uniform profile at about $\tau^* i^*_{cell} = 0.222$, and then decreases continuously with this uniform profile until the cell is totally discharged at $\tau^* i^*_{cell} = 3.7$ and it reaches 0.2. These distributions are also similarly shaped to those for the DL process alone, as shown in Fig. 2C. Meanwhile, the faradaic current (Fig. 6B) increases with time and its distribution reaches a maximum of nonuniformity at about $\tau^* i^*_{cell} = 0.222$. Finally, a uniform distribution is attained and the faradaic current reaches 0.8 at $\tau^* i^*_{cell} = 3.7$, which is four times greater than the final current for the DL process alone, as shown in Fig. 6A. For the faradaic process alone (Fig. 6C), the faradaic current distribution is at a maximum of nonuniformity at the start of discharge, then the degree of this nonuniformity decreases with time, and finally it reaches a uniform profile at $\tau^* i^*_{cell} = 2.8$.

Because local potentials are related to local currents, a change in local potential must result in a change in local current. However, for the DL and faradaic processes alone, they are related in different ways. The DL current is proportional to the derivative of the local potential with respect to time (Eq. 24), but the faradaic current is nonlinearly related to the local potential with an exponential dependence (Eq. 25 and 4). These different features for the two processes determine their different current distributions in response to a change in local potential. For the DL process alone (Fig. 2B and C), the change in local potential is the greatest at the start of discharge; as a result, the DL current distribution reaches a maximum of nonuniformity. As the change in local potential becomes smaller with time, the DL current distributions become more uniform. Finally, as the potential distribution attains a steady-state profile, the change in local potential with time is the same throughout the electrode, which leads to a uniform DL current distribution. For the faradaic process alone (Fig. 5B and 6C), the change in local potential is also the greatest at the start of discharge, which leads to a very nonuniform, faradaic current distribution; meanwhile, the potential distribution reaches a steady-state profile instantly. This steady-state potential profile does not translate into a uniform faradaic current distribution because of the nonlinear relationship between the local potential and the local current as shown in Eq. 4. The final uniform faradaic current distribution is likely reached because the difference between the two exponential terms approaches a constant. For the combined DL and faradaic processes, the potential and the DL current distributions are similar to those for the DL process alone; its faradaic current distributions are similar to those for the faradaic process alone. However, the relative magnitudes of the DL and faradaic currents are determined by how they are related in the governing equations (Eq. 4, 24, and 25).

The results in Fig. 3A show that the particle size is extremely important to the discharge behavior of the capacitor. It is therefore of interest to investigate the performance of this model capacitor in terms of Ragone plots, *i.e.*, in terms of the energy and power densities. The energy and power densities are calculated as follows

$$\text{Energy density} = \frac{I_{cell}\Phi_{ave}t_d}{V_{cell}} \quad [30]$$

$$\text{Power density} = \frac{I_{cell}\Phi_{ave}}{V_{cell}} \quad [31]$$

where I_{cell} is the total cell current, which is obtained by multiplying the cell current density (i_{cell}) by the cross-sectional area of the electrode, A. Φ_{ave} is the average cell potential, t_d is the discharge time, and V_{cell} is the volume of the cell including the electrodes, electrolyte, and separator. The average cell potential is given by

S0013-4651(98)11-057-1 CCC: $7.00

$$\Phi_{ave} = \frac{1}{t_d}\int_0^{t_d} \Phi_{cell}\, dt \qquad [32]$$

Figure 7A shows Ragone plots for the combined DL and faradaic processes and for three different particle sizes. The curves are all similarly shaped, but the energy density decreases with an increase in particle size over the entire range of power densities, and it begins to drop off sooner but more slowly as the power density increases. To examine how the DL and faradaic processes independently affect the energy and power densities in a capacitor, Fig. 7B shows the contributions from each process for a capacitor with 5 nm diam $RuO_2 \cdot xH_2O$ particles. The Ragone plots exhibit similar trends for the combined DL and faradaic processes and the DL and faradaic processes alone, except at very high powers. For the DL process alone, the energy density is essentially independent of the power density up to about 20 kW/L, and then it drops sharply at higher power densities. In contrast, the energy density decreases a little faster with an increase in power density for the faradaic process alone. At very high power densities (above 100 kW/L), however, the faradaic process fails because the potential in the positive electrode drops instantly below 0.5 V at the start of discharge, and no energy can be drawn from the cell at such high power densities. For the combined DL and faradaic processes, a higher energy density over a broader range of power densities is due largely to the faradaic process; however, it approaches the energy density obtained for the DL process alone at very high power densities, again indicating that the contribution from the faradaic process becomes negligibly small at very high power densities. Overall, these Ragone plots show very clearly that for a capacitor utilizing both DL and faradaic processes, a higher energy density results from the faradaic process and a higher power density results from the DL process, as compared to either of the individual processes alone.

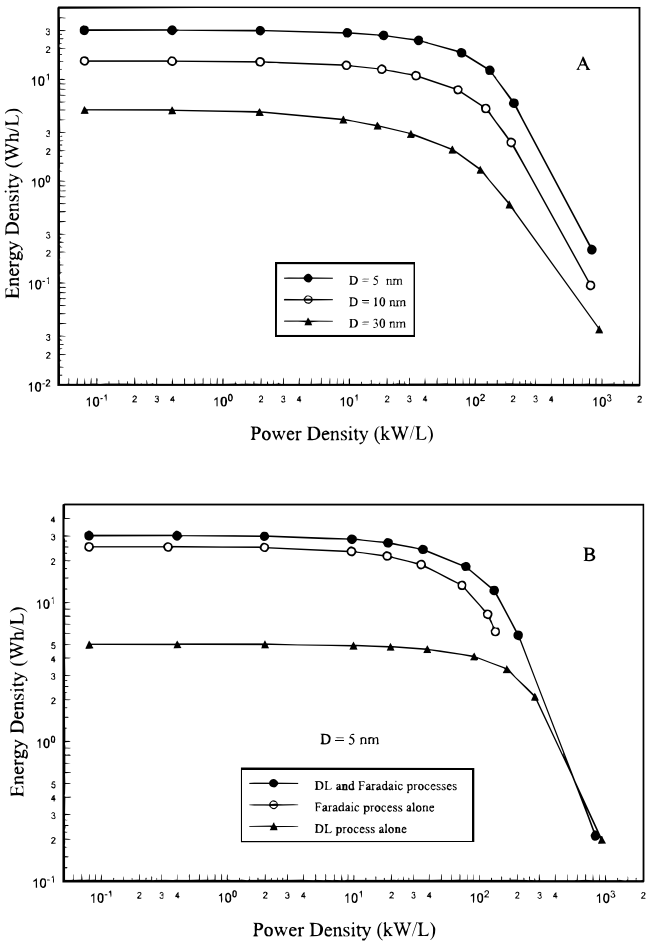

Figure 7. Regone plots: (A) for the combined DL and faradaic processes for three $RuO_2 \cdot xH_2O$ particle sizes and (B) for the DL process alone, faradaic process alone, and combined DL and faradaic processes with 5 nm diam $RuO_2 \cdot xH_2O$ particles.

Discussion

Both of the DL and faradaic processes studied here are surface phenomena which take place at the interface between the electrode and electrolyte. For the DL process, more surface area and a higher specific capacitance both give rise to more energy storage at the interface. Also, for the surface faradaic process, more surface area gives rise to more energy storage at the interface. Moreover, the more active the surface material is toward reversible redox reactions (determined by the value of the exchange current density, i_0), the higher the power density. In this study, however, the specific capacitance of the DL process and the exchange current density of the faradaic process are all fixed; so the only variable is the surface area, which is changed by varying the size of the $RuO_2 \cdot xH_2O$ particles in the electrode. In fact, some researchers[34] reported much higher DL capacitance of 60 $\mu F/cm^2$ for oxide electrode systems based on a proton-exchange mechanism. In this case, the calculated DL current would be expected to be tripled, which in turn would result in a threefold increase in the energy density contributed from the DL process.

According to Eq. 26, the surface area is inversely proportional to the particle size. As the particle size decreases from 30 to 10 to 5 nm, the surface area increases three times and six times, respectively, which is proportionally the same as the increase in the discharge times shown in Fig. 3A. In addition, the results in Fig. 3B show clearly that the discharge time for the faradaic process alone is five times higher than that for the DL process alone, indicating the importance of the faradaic process for increasing the energy density of a capacitor. Furthermore, Eq. 30 and 31 state that the energy density is proportional to the total cell current, I_{cell}, average cell potential, Φ_{ave}, and discharge time, t_d, but it is inversely proportional to the cell volume, V_{cell}. The power density is the same as the energy density except that it is independent of t_d (which may not be true because Φ_{ave} is a function of t_d). Although a first glance at these equations suggests that an increase in cell current results in an increase in energy density, actually this is not true because the discharge time decreases with an increase in cell current. The overall effect is that the energy density decreases with an increase in power density. The results in Fig. 7A show that the ratio of the increase in energy density at the same power density is roughly the same as the ratio of the increase in surface area for the three different sizes of $RuO_2 \cdot xH_2O$ particles.

In addition, in order to increase the power density, the cell current density must be increased, as shown in Fig. 7A and B. However, the resulting increase in power density is obtained at the expense of decreasing energy density, mainly because of the ohmic resistance in the solution phase for the DL process alone. For the faradaic process alone, the energy loss at higher power densities is due to the ohmic resistance in the solution phase as well as the faradaic kinetic resistance. The faradaic kinetic resistance even makes the faradaic process alone fail, because the cell potential cannot hold at the working potential range. What is even more interesting, however, is that for the combined DL and faradaic processes, the energy loss is less compared with that for the faradaic process alone at the same power density. The reason is that the DL process has the ability to hold the cell potential, which allows the faradaic process to deliver some energy even beyond the power at which the faradaic process alone would fail. These results are consistent with those shown in Fig. 2A, 4A, and 4B, which indicate that the energy loss at the larger current (based on relative utilization) is 20, 44, and 37% for the DL process alone, faradaic process alone, and combined DL and faradaic processes, respectively. Although there is always a trade-off between the energy and power densities, a capacitor with both DL and faradaic processes can store more energy and deliver more power compared with that obtained from either the DL or faradaic processes alone.

S0013-4651(98)11-057-1 CCC: $7.00

In this study, it is also assumed that the faradaic reaction takes place only at the surface of the particle with one-electron exchange between 0 and 1 V (SCE). In practice, however, the inner layers within a particle may also participate in the redox reaction through a proton diffusion mechanism;[3,10] other authors[35] have suggested a faradaic reaction of RuO_2 with a two-electron exchange. As a result, the faradaic charge of a fully oxidized electrode can double according to Eq. 27, which means that the energy density from the faradaic process can also double. Nevertheless, the power density may decrease because of slow proton diffusion in the innerlayers of the solid phase. In addition, in this study the electronic conductivity of the matrix is taken as 105 S/cm, which is 3-4 orders of magnitude higher than the value suggested by some researchers[36] based on boundary effects associated with powder materials[37] and less crystallinity[38] in hydrous RuO_2. However, if the conductivity is taken as this lower value, the simulated results will not be affected much because the limiting conductivity is in the solution.

Conclusions

A mathematical model of an electrochemical capacitor comprised of hydrous ruthenium oxide ($RuO_2 \cdot xH_2O$) electrodes, including both DL and surface faradaic processes, was developed to predict the behavior of the capacitor under the conditions of galvanostatic charge and discharge. A comparison of various numerical solutions from the model with analytical ones for the DL process alone revealed that the numerical simulations were accurate up to the fourth digit. The results show that the energy density can be increased by decreasing the particle size, whereas the power density can only be increased by increasing the cell current density. However, there is always a tradeoff between the energy and power densities. The results also indicate that a capacitor with both DL and faradaic processes has higher energy densities compared with the DL process alone and higher power densities compared with the faradaic process alone. The model predicts that the faradaic process increases significantly the energy per unit volume of the capacitor for power densities of 100 kW/L or less.

Acknowledgments

The authors are grateful for the financial support provided in part by the U.S. Army Research Office under grant no. DAAH04-96-1-0421 and in part by the U.S. Department of Energy under Cooperative Agreement no. DE-FC02-91ER75666.

The University of South Carolina assisted in meeting the publication costs of this article.

List of Symbols

A	cross-sectional area of the electrode, cm^2
C_d	DL capacitance per unit surface area, F/cm^2
D	diameter of the $RuO_2 \cdot xH_2O$ particles, cm
E	local electrode potential, $\Phi_1-\Phi_2$, V
E^*	dimensionless local potential, $E/2V_o$
f	F/RT, V^{-1}
F	Faraday's constant, 96487 C/equiv
h	length of the crystal lattice on the $RuO_2 \cdot xH_2O$ surface, cm
i_0	exchange current density for the faradaic reaction, A/cm^2
i_1	superficial current density in the matrix phase, A/cm^2
i_2	superficial current density in the electrolyte phase, A/cm^2
i_c	DL current per unit volume of the electrode, A/cm^3
i_{cell}	applied cell current density, A/cm^2
I_{cell}	total cell current, A
i^*_c	dimensionless DL current, i_cL/i_{cell}
i^*_{cell}	dimensionless cell current, $i_{cell}L(\kappa_p + \sigma)/(\kappa_p\sigma V_o)$
i_f	faradaic current per unit volume of the electrode, A/cm^3
j_f	faradaic transfer current density, A/cm^2
i^*_f	dimensionless faradaic current, i_fL/i_{cell}
L	thickness of the electrode, $L = L_+ = L_-$, cm
L_A	Avogadro's number, 6.0226×10^{23} mol^{-1}
L_s	thickness of the separator, cm
Q_f	faradaic charge per unit volume of the electrode, C/cm^3
$Q_{f,oxd}$	faradaic charge per unit volume of the fully oxidized electrode, C/cm^3
$Q_{f,red}$	faradaic charge per unit volume of the fully reduced electrode, C/cm^3
R	universal gas constant, 8.3143 J/mol K
s_v	specific surface area per unit volume of the electrode, cm^2/cm^3
t	time, s
t_d	discharge time, s
T	temperature, K
U_1	equilibrium potential for the faradaic reaction, V (*vs.* SCE)
V_{cell}	volume of the cell, cm^3
V_o	initial potential before charge, 0.5 V (*vs.* SCE)
x	position coordinate, cm

Greek

α_a	anodic transfer coefficient of the faradaic reaction
α_c	cathodic transfer coefficient of the faradaic reaction
δ	state of charge in the faradaic reaction
ϵ	electrode porosity
ϵ_s	separator porosity
Φ_1	potential in the matrix phase, V
Φ_2	potential in the electrolyte phase, V
Φ_{ave}	average cell potential, V
Φ_{cell}	cell potential or the matrix potential difference between the two current collectors, V
Φ^*_{cell}	dimensionless cell potential, $\Phi_{cell}/2V_o$
κ_0	ionic conductivity of the bulk electrolyte, S/cm
κ_p	ionic conductivity of the electrolyte inside the pores of the electrode, S/cm
κ_s	ionic conductivity of the electrolyte inside the pores of the separator, S/cm
θ	fraction of oxidized species in the faradaic reaction
σ	electronic conductivity of the matrix phase, S/cm
τ	DL time constant, s
τ^*	dimensionless time, t/τ
ξ	dimensionless position coordinate, x/L

References

1. B. E. Conway, *J. Electrochem. Soc.*, **138,** 1539 (1991).
2. B. E. Conway, in *Third International Seminar on Double Layer Capacitors and Similar Energy Storage Devices*, Vol. 3, Florida Educational Seminar, Inc., Boca Raton, FL (1993).
3. S. Trasatti and P. Kurzweil, *Platinum Metals Rev.*, **38,** 46 (1994).
4. S. Sarangapani, B. V. Tilak, and C. P. Chen, *J. Electrochem. Soc.*, **143,** 3791 (1994).
5. I. D. Raistrick, in *Electrochemistry of Semiconductors and Electrodes*, J. McHardy and F. Ludwig, Editors, pp. 297-355, Noyes Publications, Park Ridge, NJ (1992).
6. H. Shi, *Electrochim. Acta*, **41,** 1633 (1996).
7. M. Aoki, K. Sato, and Y. Kobayashi, *IEICE Trans. Fundam.*, **E77-A,** 208 (1994).
8. S. T. Mayer, R. W. Pekala, and J. L. Kaschmitter, *J. Electrochem. Soc.*, **140,** 446 (1993).
9. I. Tanahashi, A. Yoshida, and A. Nishino, *Carbon*, **29,** 1033 (1991).
10. J. P. Zhang, P. J. Cygan, and T. R. Jow, *J. Electrochem. Soc.*, **142,** 2699 (1995).
11. K. C. Liu and M. A. Anderson, *J. Electrochem. Soc.*, **143,** 124 (1996).
12. V. Srinivasan and J. W. Weidner, *J. Electrochem. Soc.*, **144,** L210 (1997).
13. C. Lin, J. A. Ritter, and B. N. Popov, *J. Electrochem. Soc.*, **145,** 4091 (1998).
14. F. A. Posey and T. Morozumi, *J. Electrochem. Soc.*, **113,** 176 (1966).
15. A. M. Johnson and J. Newman, *J. Electrochem. Soc.*, **118,** 510 (1971).
16. W. Tiedemann and J. Newman, *J. Electrochem. Soc.*, **122,** 70 (1975).
17. V. Srinivasan, C. Lin, J. A. Ritter, and J. W. Weidner, in *Electrochemical Capacitors II*, F. M. Delnick, D. Ingersoll, X. Andrieu, and K. Naoi, Editors, PV 96-25, p. 153, The Electrochemical Society Proceedings Series, Pennington, NJ (1996).
18. C. J. Farahmandi, in *Electrochemical Capacitors II*, F. M. Delnick, D. Ingersoll, X. Andrieu, and K. Naoi, Editors, PV. 96-25, p. 167, The Electrochemical Society Proceedings Series, Pennington, NJ (1996).
19. B. Pillay and J. Newman, *J. Electrochem. Soc.*, **143,** 1806 (1996).
20. O. S. Ksenzhek, Russ. *J. Phys. Chem.*, **37,** 1089 (1963).
21. S. Sarangapani, B. V. Tilak, and C.-P. Chen, *J. Electrochem. Soc.*, **143,** 3791 (1996).
22. M. Doyle, T. F. Fuller, and J. Newman, *J. Electrochem. Soc.*, **140,** 1526 (1993).
23. J. Newman and W. Tiedemann, *AIChE J.*, **21,** 25 (1975).
24. P. De Vidts and R. E. White, *J. Electrochem. Soc.*, **144,** 1343 (1997).
25. T. R. Jow and J. P. Zhang, *J. Electrochem. Soc.*, **145,** 49 (1998).
26. T. Yeu and R. E. White, *J. Electrochem. Soc.*, **137,** 1327 (1990).
27. R. E. White, S. E. Lorimer, and R. Dardy, *J. Electrochem. Soc.*, **130,** 1123 (1983).
28. M. E. Davis, *Numerical Methods and Modeling for Chemical Engineers*, John Wiley & Sons, New York (1984).
29. J. S. Newman, *Electrochemical Systems*, 2nd ed., Prentice-Hall, Inc., Englewood Cliffs, NJ (1991).
30. K. Kimoshita, *Carbon: Electrochemical and Physicochemical Properties*, John Wiley & Sons, New York (1988).
31. F. H. Pollak and W. E. O'Grady, *J. Electrochem. Soc.*, **132,** 2385 (1985).
32. S. Trasatti and G. Lodi, in *Electrodes of Conductive Metallic Oxides-Part A*, p. 301, S. Trasatti, Editor, Elsevier, New York (1980).
33. H. E. Darling, *J. Chem. Eng. Data*, **9,** 421 (1964).
34. S. Levine and A. L. Smith, *Disc. Faraday Soc.*, **52,** 290 (1971).
35. D. Michell, D. J. A. Rand, and W. Woods, *J. Electrochem. Soc.*, **89,** 11 (1978).
36. S. Pizzini, G. Buzzanca, C. Mari, L. Rossi, and S. Torchio, *MRS Bull.*, **7,** 449 (1972).
37. S. Trasatti, *Electrochim. Acta*, **36,** 225 (1991).
38. W.-C. Shin and S.-G. Yoon, *J. Electrochem. Soc.*, **144,** 1055 (1997).